Understanding the interplay between electrocatalytic C(sp³)–C(sp³) fragmentation and oxygenation reactions

*Christine Lucky[1], Shengli Jiang[1], Chien-Rung Shih[1], Victor M. Zavala[1], and Marcel Schreier[1,2]**

[1] Department of Chemical and Biological Engineering, University of Wisconsin-Madison, Madison, Wisconsin 53706, United States

[2] Department of Chemistry, University of Wisconsin-Madison, Madison, Wisconsin 53706, United States

AUTHOR INFORMATION

Corresponding Author

* Prof. Marcel Schreier

Department of Chemical and Biological Engineering & Department of Chemistry

University of Wisconsin – Madison

1415 Engineering Drive, Madison, WI 53706

E-mail: mschreier2@wisc.edu

ABSTRACT

Achieving the selective electrocatalytic activation of $C(sp^3)-C(sp^3)$ and $C(sp^3)-H$ bonds is key to enabling the electricity-driven synthesis of chemicals, the sustainable upgrading of plastics, and the development of fuel cells operating on energy dense liquid fuels. When exposed to electrodes under oxidative bias, hydrocarbons undergo both C−C bond fragmentation and oxygenation. Currently, we lack control over the bifurcation between these pathways. Herein, we provide insight into the complex network of alkyl-transformation reactions, showing that under oxidizing potentials, adsorbed butane transforms to $*CH_x$ fragments which can be desorbed as methane before oxidizing to *CO. Identifying the branchpoint between C–C fragmentation and oxygenation allows us to steer selectivity by applying pulsed potentials tailored to the desorption potential of specific adsorbates and the timescale of intermediate oxidation. Our findings provide design criteria for improved fuel cell catalysts and open the door to selective C–C cleavage in electrosynthetic pathways.

Introduction

Mitigating climate change will require widespread decarbonization of chemical synthesis, energy generation and energy storage.[1–5] Electrocatalysis is key to realizing this vision, as it forms a natural bridge between the chemical and renewable electricity value streams by intimately linking chemical reactions to electron flow.[3,6] Decarbonization efforts will have to include the electrification of carbon intensive processes such as plastics synthesis and recycling,[7–10] biomass upgrading,[11–13] and fine chemical synthesis,[14–17] as well as the recovery of energy from chemicals in fuel cells.[18,19] All of these reactions involve the transformation of $C(sp^3)$–H and $C(sp^3)$–$C(sp^3)$ bonds, which are ubiquitous in plastics, alkanes, and alcohols. Understanding the electrocatalytic activation and transformation of these bonds is therefore necessary to drive comprehensive electrification efforts.

Despite reports of electrochemical alkane oxidation dating back to the 1960s, the surface reactivity which governs alkyl fragment transformations remains poorly understood.[20–28] This is because the complex combination of dehydrogenation, C–C scission, and oxygenation steps required for oxidation present a wide range of possible pathways and intermediates.[29–31] Understanding and manipulating the interplay between these elementary steps opens the door to improved alkane and alcohol fuel cell catalysts and new reactivities. Fuel cells which run on energy dense liquid fuels, such ethanol and butanol, require both C–C bond fragmentation and oxidation.[31,32] Yet, it remains unclear which of the two processes limits fuel cell performance.[29–34] Identifying the pathway of alkyl fragment oxidation is thus a critical prerequisite for the rational design of improved catalysts. At the same time, the relevance of this mechanistic understanding transcends fuel cell applications. For example, promoting fragmentation while suppressing oxidation opens pathways to the sustainable upcycling of plastics.

Previous studies have suggested the formation of two general types of surface species upon adsorption of alkanes to platinum electrodes, which are distinguished by their ability to be desorbed under reductive conditions. The cathodically desorbable fraction may be removed as saturated alkanes under reducing conditions or as CO_2 under oxidative conditions, whereas the non-cathodically desorbable fraction can only be removed through total oxidation to CO_2.[22,35–39] While there is some insight into the nature of adsorbates formed by alkane adsorption to the electrode, we lack an understanding of how the potential controls the subsequent transformation of these species on the surface.

Herein, we employ real-time changes of the applied potential to steer the transformation of intermediates after they are bound to the catalyst surface, leading to an understanding of electrochemical alkane binding, C–C bond scission, and fragment oxidation, using butane on platinized Pt as a model system (**Figure 1**).[40] These measurements are enabled by electrochemical mass spectrometry (EC-MS), which allows for the detection of submonolayer quantities of desorbing compounds.[41,42] To facilitate the challenging analysis of long-chain alkane mixtures using mass spectrometry, we developed a deconvolution method based on sparse matrices to reliably quantify the products of butane surface reactivity as a function of time and potential. Our data show how the selectivity between fragmentation and oxidation is controlled by the relative rates of C−C scission and $*CH_x$ oxidation, which can be tuned through the applied potential program. We provide insight into the complex interplay of dehydrogenation, C−C scission, and oxygenation in the surface transformations of alkyl fragments that will provide a roadmap to the design of catalysts for efficient energy storage and the electrification of industrial reactions.

Results

Monitoring reactivity with electrochemical-mass spectrometry

To investigate the parameters controlling C−C bond fragmentation in butane, we monitored the products desorbing from a platinized Pt electrode in real time while modulating the applied potential. Platinized Pt was used to increase the surface area available for adsorption and lower the average coordination number of the surface atoms, which have been suggested to generate a more active catalyst for alkane adsorption and transformation.[43,44] Indeed, the presence of a pre-peak during CO oxidation indicates that undercoordinated sites, such as defects and step sites, are formed (Supplementary Figure 1).[43,45–47] Furthermore, the disappearance of the CO oxidation pre-peak when CO adsorption is preceded by butane adsorption supports the notion that alkanes preferentially adsorb on these undercoordinated sites (Supplementary Figure 1). Aqueous 1 M $HClO_4$ was used as electrolyte and all potentials are reported *vs* the reversible hydrogen electrode (RHE). We studied the electrochemical transformation of alkyl adsorbates by first adsorbing butane for 15 min, then removing the remaining substrate from the cell by flowing helium for 15 min at the same potential. We manipulated the pre-adsorbed compounds through modifications of the electrode potential and subsequently desorbed products through application of reductive and

oxidative potentials, while quantifying them using mass spectrometry. The mass fragments detected during oxidative desorption were characteristic of CO_2. However, determining the identity of alkanes desorbed under reducing conditions necessitated additional processing to deconvolute the overlapping mass fragments formed during ionization in the mass spectrometer (Supplementary Figures 2&3). The conversion of ionic currents from EC-MS to the composition of species in the desorbed alkane mixture was made possible by data science. We expressed the transformation of six mass-to-charge ratios (m/z = 15, 16, 30, 43, 44 and 58) to five species (CH_4, C_2H_6, C_3H_8, C_4H_{10} and CO_2) as a constrained least squares optimization problem with ℓ_1-normalization, which was solved using a trust region algorithm.[48]

Potential-dependence of butane adsorption and desorption

To understand the chemical transformations that surface-bound butane undergoes in response to the applied potential, we first needed to understand how butane adsorbs under electrochemical control. To this end, we adsorbed butane at potentials between 0.2 to 0.7 V and quantified the amount of CO_2 generated upon sweeping the potential to oxidizing conditions (**Figure 2a**). Butane adsorption reached a maximum at 0.3 V and decreased at more oxidative and reductive potentials (**Figure 2b**). This behavior is consistent with previous voltammetric studies of alkane adsorption on Pt, which find a maximum at 0.25 – 0.4 V *vs* RHE, near the potential of zero charge (PZC).[22,28,35,49–51] The maximum in adsorption has been hypothesized to occur in the vicinity of the PZC because it is easier for the uncharged alkanes to displace dipolar water and ions on a minimally charged electrode.[22,43,44,52,53]

After characterizing the potential dependence of butane adsorption, we directed our attention to the composition of the resulting adsorbed species. Applying 0.05 V after butane adsorption initiated the release of reductively desorbable species, resulting in the detection of potential-dependent mixture of butane and methane. We found that more oxidative adsorption potentials promoted C–C scission but reduced the overall selectivity toward reductively desorbable compounds (**Figure 2c**). After adsorption at 0.2 V, butane was the only reductively desorbed product. However, adsorption at more positive potentials led to the appearance of small amounts of methane (**Figure 2d**), indicating that C–C scission takes place. Importantly, we did not observe alkanes of intermediate chain length. This absence was also observed using propane

(Supplementary Figure 4) and is consistent with alkene oxidation literature which reports the cathodic desorption of only methane and propane following propylene adsorption.[54] The detection of only C_1 cracking products is interesting as it suggests that on Pt, alkyl fragments either undergo total C–C scission or form methane precursors along with non-reductively desorbable residues. This differentiation is of great importance for the oxidation of hydrocarbons and alcohols in fuel cells, where the formation of strongly bound, non-desorbable compounds could decrease catalyst performance. Distinguishing between these mechanisms requires insight into the chemical identity of the surface species formed upon butane adsorption.

Butane adsorption leads to three distinct surface compounds

We determined that butane forms three distinct surface intermediates on Pt by combining voltammetric measurements with real-time product analysis. In a first step, we analyzed the current generated by the oxidation of adsorbed butane during an oxidative potential sweep and compared it to that of a bare surface (**Figure 3a**). We observed three oxidation peaks corresponding to the total oxidation of butane-derived adsorbates. These peaks, labelled I, II_a, II_b and III, occur at 0.71, 0.84, 1.05 and 1.33 V respectively (**Figure 3b**). Peaks II_a and II_b, arise from a single broad peak that is split as a result of background subtraction and is treated herein as a single oxidation process (see Supplementary Figure 5).[27] The onset of CO_2 generation coincided with the onset of the first oxidation peak at 0.58 V (**Figure 3b**) and subsequent experiments confirmed that CO_2 generation accompanied all other peaks (Supplementary Figures 6&7).

We then sought to establish which voltammetric oxidation peaks correspond to reductively desorbable compounds. To identify these species, we repeated our oxidative stripping experiments after first removing reductively desorbable compounds at 0.05 V. We found that only peaks I and III remained after reductive desorption (**Figure 3b**), leading us to conclude that oxidation of the reductively desorbable species generates peak II.

Assignment of chemical structures to surface adsorbates

To assign a chemical structure to the compound undergoing oxidation at peak II, we measured the oxidation state of the carbon atoms. We calculated this value by determining the number of electrons needed to produce one molecule of CO_2 from the total oxidation of adsorbates, which we refer to as N (**Equation 1**).[24,36,55,56]

$$N = \frac{n_{e^-}}{n_{CO_2}} \quad (1)$$

The validity of this approach was verified by oxidizing a monolayer of CO, which required 2.1 electrons per CO molecule, close to the theoretical N value of 2 (Supplementary Figure 8). These measurements of N values allowed us to determine that peak II likely arises from an intact butyl fragment. The desorption of species II as butane suggests that the adsorbate has not undergone C–C cleavage. Dissociative binding of butane through the replacement of one C–H bond with a C–Pt bond yields an adsorbate with an N value of 6.25 (see SI), which is close to our measured value of 6.4 at 0.2 V. At higher adsorption potentials, we observed a decrease in the N value, indicating a transition to a 4-site binding mode, as has been previously suggested (Supplementary Figure 9).[22,25]

Based on similar measurements of N values, we determined that peak I corresponds to an oxygenated species. We isolated species I by adsorbing butane at 0.4 V and reductively removing species II prior to partial oxidative stripping (Supplementary Figure 10). Oxidation of species I led to an N value of 3.2. This indicates the presence of an oxygenated species as N values below 4 are only possible if an oxygen atom is present in the adsorbate (**Table 1**).[24,38] The experimental N value is consistent with a *CHO or *COH adsorbate, but further investigations allowed us to assign peak I to adsorbed carbon monoxide (*CO). As discussed in the mechanistic section, species I is continuously generated during the stripping experiment, resulting in additional electrons being passed. Therefore, the true N value for species I is likely lower than the measured value of 3.2.

Comparing the oxidative stripping of species I to model compounds allowed us to overcome uncertainty in the oxidation state calculations and indicated that peak I arises from the oxidation of *CO. The oxidative current and CO_2 generation associated with the total oxidation of species I aligned with those obtained after methane adsorption under the same conditions, suggesting that peak I arises from a C_1 adsorbate (Supplementary Figure 11). Previous studies report that methane forms *CO upon adsorption on platinized Pt, allowing us to assign species I.[43,44,56] The attribution of peak I to *CO was further supported by CO-stripping experiments where the oxidation of species I and onset of the first oxidative stripping feature of *CO occurred at the same potential (Supplementary Figure 11).[24,38] Our findings are consistent with the non-cathodically desorbable CO-like[57] and reduced CO_2[58] species previously proposed.[27]

The oxidation state of species III cannot be independently quantified because it undergoes conversion at potentials below its total oxidation (Supplementary Figure 12). However, based on similarities to species involved in ethylene and propylene electrooxidation, we speculate that it

could correspond to an oxygenated C_4 species.[54,59,60] It cannot be excluded that peaks II and III correspond to the same species on two different surface sites which have different propensities for reductive desorption and distinct onset potentials for total oxidation.

Influence of adsorption potential on surface species formed

To steer the transformation of organic compounds on electrode surfaces after adsorption, we first need to understand the nature of the butane adsorbates under equilibrium conditions. We did this by performing oxidative stripping following adsorption at 0.2 - 0.7 V and found that at more oxidative adsorption potentials the proportion of adsorbed *CO increased and the coverage of reductively desorbable butyl fragments decreased. Specifically, butane adsorbed at 0.2 V formed predominantly 4-carbon adsorbates which could be removed at reductive potentials (Supplementary Figure 13). As the adsorption potential increased from 0.2 V to 0.5 V, peak I increased while peak II decreased, implying the formation of *CO at modest potentials. This shift agrees with the observed increase in non-cathodically desorbable species across the same potential range (**Figure 2c**). At adsorption potentials above 0.5 V, we observed the disappearance of peak I, which we attribute to the continuous oxidation of *CO to CO_2, resulting in its continuous removal from the surface (Supplementary Figure 3).[61,62] The presence of *CO at mildly oxidative potentials indicates that C−C bond scission is not solely the result of a reductive potential excursion as previously reported for alkene oxidation.[63] Since *CO is not removed from the surface by reductive desorption, we attribute methane generation to another species. However, the low yield of methane prevented the direct identification of its associated adsorbate through oxidative stripping. To shed light onto the methane generation pathway, we next studied the mechanistic origin of C−C bond fragmentation.

Oxidative potentials convert C_4 species to CH_4 precursors

To study the potential driven transformation of butyl fragments leading to methane, we needed to isolate the fragmentation step from butane adsorption. We did this by adsorbing butane at 0.2 V, where no methane production was observed, then increasing the voltage to 0.5 V for varying durations to induce cracking.[40] Following the 0.5 V hold with a reductive potential pulse allowed us to quantify the reductively desorbable products. We complemented these measurements with oxidative stripping experiments which omitted the reductive step and provided voltammetric information about all species present on the surface (**Figure 4a**). These experiments allowed us to develop a detailed picture of how different surface adsorbates transform under an

applied potential and indicated that methane is generated from an intermediate product during these transformations.

The application of a 0.5 V hold induced methane generation, demonstrating that changes to the potential after adsorption can steer the electrocatalytic reactivity of butane. The generation of methane was accompanied by a decrease in butane. However, only a small portion of the disappearing butane could be accounted for by methane production, indicating that a majority of the butane precursor reacts to form a different product, which is likely *CO (Supplementary Figures 14-16). Indeed, oxidative stripping experiments showed an increase of *CO on the surface during the 0.5 V hold. The rise in peak I was accompanied by a decrease in peak II, providing further evidence that butane precursors convert to *CO at 0.5 V (**Figure 4c**). While the transformation of butane precursors to *CO emerges clearly, it remained unclear which surface species leads to the release of methane under reductive conditions.

Interestingly, the emergence of peak I is correlated with increased methane yield. Yet, it is unlikely that *CO is the species leading to methane as it remains on the surface after cathodic desorption (**Figure 3b**). Rather, we hypothesize that the conversion of C_4 adsorbates to *CO involves a short-lived intermediate which can be desorbed as methane. This notion is supported by the asynchronous consumption of butane and generation of methane (**Figure 4b**). While butane decreased across the entire range of hold times, methane production increased sharply over the first 15 min before leveling out, suggesting that the methane yield is limited by a further reaction of the methane precursor. Such a mechanism would imply that the selectivity toward methane generation is dictated by the relative rates of C–C bond cleavage and methane precursor decomposition on the surface.

Still, the question remained if the adsorbed butyl fragment was the only species that undergoes C–C cleavage leading to methane. To determine if species III also produces methane, we investigated its reactivity in isolation. We did this by adsorbing butane at 0.4 V then removing the butyl fragments through reductive desorption at 0.05 V to leave only non-cathodically desorbable surface species. The applied voltage was then alternated between oxidative pulses of increasing potential from 0.2 to 0.7 V and reductive desorption at 0.05 V (Supplementary Figure 17) to identify the potentials leading to methane generation. Methane was observed to form from species III after holds at 0.4 V or higher showing that the non-cathodically desorbable multi-carbon

species also produces methane precursors under the application of a sufficiently oxidative potential. Furthermore, the amount of desorbed methane increased with an increase in the applied potential suggesting that the rate of cleavage is potential dependent. We therefore expect that tuning the magnitude, duration, and number of oxidative potential steps will control the yield of desorbed methane.

Proposed pathway of methane generation from C−C scission

We find that butyl fragments (species II) and the proposed C_4 oxygenate (species III) likely generate methane through a similar pathway, wherein oxidative potentials promote C−C cleavage to form *CO. Oxidative stripping experiments show that both species slowly convert to *CO at potentials associated with methane generation (**Figure 4c** and Supplementary Figure 12). This oxidation of the C_4 adsorbates occurs slowly and the consumption of butyl surface species remained incomplete after 60 min at 0.5 V (**Figure 4b**). However, methane desorption plateaued much more rapidly, after 15 min, suggesting the methane precursor does not simply accumulate on the surface. Based on this data, we theorize that methane is generated from a *CH_x intermediate formed after C−C scission, which continuously gets oxidized to *CO, but can be desorbed in the form of methane if a reductive potential is applied prior to its oxygenation (**Figure 5**). Performing desorption of this *CH_x intermediate in a deuterated electrolyte did not allow for quantification of the oxidation state of the intermediate as it resulted in the observation of fully deuterated alkanes (Supplementary Figure 18). This finding is consistent with previous reports which suggest that the C−H bonds are labile compared to the C−C bonds.[21] Additionally, we cannot exclude the possibility that oxidative potentials promote the formation of a similarly short-lived multicarbon intermediate which undergoes C−C cleavage at reductive potentials to produce methane. In either case, the relative rates of intermediate formation and further oxidation to *CO govern the selectivity between oxidation and fragmentation. Our results indicate that these steps display unique potential dependence allowing the reaction to be controlled through the applied voltage.

Increasing the methane yield using pulsed potentials

Gaining precise control over surface reaction processes has the potential to open thus far uncharted avenues of steering catalytic reactivity. Using our insight into the methane generation pathway, we were able to rationally design potential sequences that specifically interact with the

kinetic network to increase the methane yield by selectively desorbing methane over butane, while mitigating the formation of *CO. In our hypothesized pathway, *CO is formed by the oxygenation of $*CH_x$ methane precursors at potentials which induce fragmentation. Thus, decreasing the duration of the fragmentation step should decrease the amount of *CO generated. However, short fragmentation times lead to low butane conversion, as most of the substrate is desorbed in its unreacted form (Supplementary Figure 19). Converting a larger fraction of the substrate is desirable, but doing so requires a way to selectively desorb methane from the surface while retaining butyl species on the catalyst.

To identify a route to selectively desorb methane, we first compared the potential-dependent adsorption of methane on a platinized Pt electrode to that of butane. We found that methane adsorbs to a lesser extent and across a narrower potential range than butane (Supplementary Figure 20). This deviation suggested that there may be a potential range at which methane, but not butane, is desorbed. To identify this region, we adsorbed and fragmented butane at 0.4 V before incrementally lowering the potential from 0.2 V to −0.02 V to induce desorption (Supplementary Figure 21). We found that methane was selectively desorbed between 0.08 and 0.16 V without removing butane from the surface (**Figure 6**).

Having identified conditions that promote selective methane desorption, we sought to increase the methane yield by tuning the kinetic pathways to limit $*CH_x$ overoxidation. This was accomplished by subjecting the surface species to multiple fragmentation-desorption cycles using a pulsed potential profile. Pulsed potentials have gained interest for a wide range of chemistries including CO_2 reduction, formic acid oxidation, and biomass valorization.[64–70] In many implementations they are used to increase the rate of reactions which also occur at constant potential by removing poisoning species. These effects have previously been leveraged to improve the rate of total oxidation of alcohols and alkanes to CO_2.[71–73] Recently, pulsed electrolysis was used to increase the selectivity toward partially oxidized products during glycerol oxidation by promoting product desorption and preventing overoxidation through the inclusion of lower potential steps.[67] Here we implemented a similar strategy to limit the overoxidation of $*CH_x$ fragments to *CO and recover them as methane. In our sequence, shown in **Figure 7a,** butane was first adsorbed at 0.3 V. Then, the potential was alternated between a fragmentation step ranging between 0.4 and 0.7 V and a short methane desorption step at 0.1 V to desorb the transiently

formed C_1 surface species. Using a desorption potential of 0.1 V allowed us to selectively recover methane from the surface without removing butyl species that can undergo fragmentation in subsequent cycles. In this way, both butane conversion and methane yield were increased as C_4 adsorbates were subjected to multiple scission steps, and the resulting $*CH_x$ fragments were desorbed before being oxidized to *CO (Supplementary Figure 22).

We found that oscillating the potential to induce C–C fragmentation and rapid desorption yielded substantially more methane than the corresponding single step experiments for potentials between 0.4 and 0.7 V (**Figure 7b**). This was true for sequences using either a 30 s or 60 s fragmentation step followed by a 60 s methane desorption step, denoted as *30s-60s* and *60s-60s* respectively. For fragmentation potentials up to 0.6 V, the methane yield increased with the applied potential. A maximum of 6.5 nmol cm^{-2} of methane was produced using the *60s-60s* condition at 0.6 V, which is nearly an order of magnitude higher than the single step maximum of 0.71 nmol cm^{-2} (**Figure 7c**). When further increasing the fragmentation potential to 0.7 V, the methane yield decreased, likely due to the increasingly favorable oxidation reaction depleting the surface C_4 species available for fragmentation in later cycles. While more oxidative fragmentation potentials increased the methane yield up to 0.6 V, they resulted in a lower selectivity toward methane due to more CO_2 being produced (Supplementary Figures 23-25). These findings are consistent with our proposed reaction pathway and underscore the importance of controlling the relative rates of $*CH_x$ generation through fragmentation and its subsequent oxidation to *CO.

To show that the distinct potential dependence and kinetics of C−C bond scission and fragment oxygenation can be leveraged to produce methane from butane with high selectivity, we lowered the fragmentation potential and increased the duration of the fragmentation step. We found that applying 0.4 V inhibited *CO formation to a greater extent than C−C bond scission, allowing $*CH_x$ fragments to accumulate on the surface. We therefore extended the fragmentation hold to 600 s, after which we desorbed methane at 0.1 V for 180 s before repeating the cycle. Using this sequence, we increased the methane yield by an order of magnitude compared to the maximum yield observed at static potentials, while maintaining 20% selectivity toward methane (Supplementary Figure 26). Eliminating all residual butane after adsorption by exchanging the electrolyte did not alter the methane yield or selectivity (Supplementary Figure 27), indicating that the increase in methane is not due to the continuous adsorption of spurious butane. Instead, the

improved methane production is the result of complete butane conversion at higher selectivity. Importantly, the identified conditions can be directly transferred to a system where butane constantly saturates the solution to achieve continuous butane transformation with the repeated desorption of constant amounts of methane (**Figure 7d**). These results demonstrate how understanding the kinetic reaction network enables the rational manipulation of individual elementary steps through the applied potential to control reaction activity and selectivity.

Discussion

We expect that the selectivity between different products from surface alkyl compounds could be further steered by tuning the reaction temperature and the microenvironment though electrolyte variation. Understanding the selectivity branch point between fragmentation and oxidation also provides insights for catalyst design. Our work suggests that on Pt, a large fraction of alkyl fragments are oxidized to *CO, limiting the yield of methane. Suppressing this oxygenation, while promoting C−C scission is necessary to favor fragmentation. We hypothesize that this can be achieved using catalyst materials with a higher predicted turnover frequency for ethane hydrogenolysis, such as Ni or Rh.[59] Varying the catalyst material is also likely to influence the site-selectivity and extent of fragmentation in long-chain alkanes, which could provide an avenue for electrochemical polyolefin recycling.

The distinct potential dependence of adsorbate formation and their subsequent transformation results in two oxidation potential regimes, which feature different rate-limiting steps (**Figure 6**). Between 0.3 and 0.5 V we observe an accumulation of *CO, implying that the oxidation of *CO to CO_2 is the rate limiting step of alkane oxidation. This suggests that the onset potential of alkane oxidation could be reduced by alloying Pt with more oxophilic metals such as Sn and Ru, as is seen in CO oxidation literature.[74–78] However, at potentials of 0.6 V and higher, the oxidation of *CO is facile and C−C scission limits overall performance. We therefore anticipate that catalysts which demonstrate high rates for both oxygen evolution and thermal hydrogenolysis, such as Ir-based electrodes, may increase activity at higher potentials.[79–81] Alloys of oxophilic metals within hosts that feature high fragmentation activity are also good candidates for fuel cell catalysts. Further investigations into the mechanism of both C−C fragmentation and oxygenation, as well the influence of potential on each elementary step, are necessary to develop precise electrocatalytic approaches for alkyl fragment transformations.

The development of reactivities to activate the inert $C(sp^3)-C(sp^3)$ and $C(sp^3)-H$ bonds in plastics, alkane fuels, and alcohols is key to building a Net-Zero hydrocarbon economy. However, the potential driven transformations of alkyl species on the electrode surface which control this reactivity have been underappreciated, impeding electrification efforts. Specifically, the lack of insight into the bifurcation between C−C bond fragmentation and oxidation hinders fuel cell catalyst design and efforts to leverage electricity for sustainable chemical synthesis. Here, we use time-dependent electrode potential sequences, combined with monolayer-sensitive EC-MS, to generate insight into the complex network of alkyl-transformation reactions connecting C−C fragmentation and oxygenation. Our findings show that the relative rates of $*CH_x$ formation and its subsequent oxidation govern the selectivity between these two processes.

Studying reaction networks through time-dependent electrode potential sequences provides unique insights into the progression of adsorbed intermediates through a reaction pathway. Our mechanistic understanding will inform the design of improved catalysts to enable fuel cells operating on energy dense liquid fuels and lay a foundation for selective C–C cleavage in electrosynthetic pathways. Tuning the rates of individual reaction steps through potential manipulation and materials engineering opens the door to complex reactivities, such as polyolefin recycling and partial oxidation. Our results thus provide a framework for expanding electrification efforts to a wide range of hydrocarbon transformations, laying the foundation for a sustainable chemical industry.

Methods

Preparation and Characterization of Platinized Pt Catalyst. Nanoporous Pt was deposited on a polished and rinsed 5 mm diameter Pt insert (0.196 cm^2 geometric area) using a chronopotentiometric approach.[82] A solution of 72 mM H_2PtCl_6 (99.9% trace metals basis, Sigma Aldrich) and 0.13 mM $Pb(C_2H_3O_2)_2$ (99.999% trace metals basis, Sigma Aldrich) in Milli-Q water was contacted with the Pt stub and −10 mA/cm^2 was passed for 10 min using a Pt wire (99.999%, Sigma Aldrich) as the counter electrode. The platinized electrode was then gently rinsed with Milli-Q water before use. Following the standard electrochemical cleaning procedure described below, the surface was free of lead and chlorine impurities within the detection limits of XPS (Supplementary Figure 28). When performing cyclic voltammetry in 1 M $HClO_4$, a broad hydrogen under potential deposition (H-UPD) peak was observed, suggesting a distribution of surface sites without a dominant facet present (Supplementary Figure 29). The electrochemical surface area (ECSA) was measured by the underpotential deposition of a Cu monolayer at 0.2 V

for 3 min using 5 mM $CuSO_4$ in 1 M $HClO_4$ followed by oxidation using a linear sweep up to 1.2 V at 20 mV/s. The background-subtracted oxidation currents were integrated to give the charge passed, which was converted to the surface area using 420 μC cm^{-2} as the correlation (Supplementary Figure 30).[83] The calculated ECSA was 73.8 cm^2, which agrees with an ECSA of 72.5 ± 1.65 cm^2 measured by CO stripping (Supplementary Table 2). The coverage of butane-derived surface species ranged from 3-16% and was calculated assuming that each carbon atom occupies one CO-binding site (Supplementary Figure 31).

EC-MS Measurements. All experiments were performed using a Biologic SP-200 potentiostat and a three-electrode assembly consisting of a platinized Pt working electrode, Pt wire counter electrode, and Ag/AgCl (3 M KCl) reference electrode. To improve stability a 100 Ω resistor was added in series before the working electrode. 1 M $HClO_4$ was used as the electrolyte. Prior to cell assembly the PTFE cell was cleaned using piranha (85% H_2SO_4, 15% H_2O_2) and the electrolyte was degassed by He sparging for 10 min. For all experiments the working electrode was cleaned by applying 1.3 V for 5 min followed by 5 cyclic voltammetry cycles between −0.1 and 1.4 V at a scan rate of 20 mV/s. A typical experiment involved butane adsorption for 15 min followed by 15 minutes under helium flow to remove residual gaseous butane. Oxidative stripping was performed by increasing the potential to 1.4 V at 5 mV/s. A chip based electrochemical mass spectrometer (Spectro Inlets, Denmark) allowed species generated at the electrode surface to diffuse through the chip and into the MS, enabling real-time detection of desorbed products (Supplementary Figure 32). The EC-MS was operated using Zilien software (Spectro Inlets).

Quantification of EC-MS Data. Each spectrum x had six data points at each time (encoded in a vector of $\mathbb{R}^6$), with each point representing the intensity of a given mass-to-charge ratio (i.e., m/z=15, 16, 30, 43, 44 and 58). The sampling rate for each spectrum is 1.2-2.1 seconds. By collecting T spectra, we obtained a data matrix $X \in \mathbb{R}^{T\times 6}$. In this study, we focused on using these spectra to quantify the flux of five species: methane (CH_4), ethane (C_2H_6), propane (C_3H_8), butane (C_4H_{10}), and carbon dioxide (CO_2). We measured the standard reference spectrum for each of these gases and combined them into a reference matrix $A \in \mathbb{R}^{6\times 5}$.

To focus only on the gases produced by the electrocatalytic reaction, we needed to remove the baseline spectrum (the background). We did this by taking the average of 180 seconds of a steady-state spectra taken under He as the baseline spectrum, $x_b \in \mathbb{R}^6$, for each experiment. We then subtracted this baseline spectrum from the original spectrum at each time point and took the rolling average in time using a window of size 10 to reduce random noise. Supplementary Figure 33 shows the spectra before and after preprocessing.

At each time point, we sought the solution to an optimization problem that could be expressed as a constrained least squares with ℓ_1-normalization:

$$\min_w \|Aw - x\|_2^2 + \lambda\|w\|_1 \quad (2)$$
$$s.t. w_i \geq 0 \text{ for } i = 1, \cdots, 5$$

where $w \in \mathbb{R}^5$ represents the flux of each gas. We aimed to minimize the difference between the predicted spectrum, Aw, and the observed spectrum x. To avoid overfitting and promote accurate quantification of the most dominant species, we used ℓ_1 -normalization to force small gas fluctuations that we attributed to measurement noise to 0. The parameter λ determines the strength of normalization, which we refer to as the sparsity ratio. Furthermore, we imposed bounds on the predicted fluxes w to ensure that they are nonnegative, as negative fluxes are not physically meaningful. The optimization problem was solved using Python and the SciPy library with a trust region algorithm.[48]

All results reported here were calculated using a sparsity ratio of $1x10^{-4}$. This value of λ was selected to minimize calculated fluxes arising from measurement noise while preserving sensitivity. To tune λ, we tested values between 0 and 10^{-5} for three experiments involving methane, butane, and CO adsorption. For these experiments, we increased the λ value until nonphysical signals, for example propane during methane experiments, were eliminated (Supplementary Figures 34&35). The signal reconstructions and calculated fluxes were then compared to the results obtained with a sparsity parameter of 0 to ensure that no significant features of the spectra were lost.

Oxidation state calculations. The number of electrons needed for total oxidation of the adsorbate to CO_2, denoted as N, was calculated using the following equation:

$$N = \frac{n_{e^-}}{n_{CO_2}} \tag{3}$$

where n_{e^-} is the number of faradaic electrons passed during oxidative stripping and n_{CO_2} is the number of CO_2 molecules produced. These values were calculated by integrating the current and CO_2 flux during the first cycle of the desorption cyclic voltammogram and subtracting the current or CO_2 produced during the corresponding blank performed under He to correct for solvent reorganization current and any organic impurities. Calculations of the N value for only the species giving rise to peak I were done by performing reductive desorption prior to the oxidative stripping and only increasing the voltage to 0.95 V to prevent the total oxidation of peak III (Supplementary Figure 6).

DATA AVAILABILITY

Experimental raw data underlying the results and conclusions of this work are publicly available at DOI: 10.5281/zenodo.12801616.

CODE AVAILABILITY

The code used to transform ionic current data to species fluxes are publicly accessible at DOI: 10.5281/zenodo.12801616.

ACKNOWLEDGMENTS

We thank Megan Kelly for input. This work was supported by the Arnold and Mabel Beckman Foundation through a Beckman Young Investigator Award (https://dx.doi.org/10.13039/100000997) (M.S.). We also acknowledge summer salary support from an NSF CAREER award (CBET-2338627) (M.S.) and the use of facilities and instrumentation at the UW-Madison Wisconsin Centers for Nanoscale Technology partially supported by the NSF through the University of Wisconsin Materials Research Science and Engineering Center (DMR-1720415). This material is based upon work supported by the National Science Foundation Graduate Research Fellowship Program under Grant No. DGE-1747503 (C.L.). Any opinions, findings, and conclusions or recommendations expressed in this material are those of the authors and do not necessarily reflect the views of the National Science Foundation. Support was also provided by the Graduate School and the Office of the Vice Chancellor for Research and Graduate Education at the University of Wisconsin-Madison with funding from the Wisconsin Alumni Research Foundation (C.L.).

AUTHOR CONTRIBUTIONS

C.L. and M.S conceived the project. C.L. designed and performed the experiments. C-R.S. assisted with data collection. S.J. developed the mass spectrum deconvolution methodology and code with assistance from C.L and V.M.Z. C.L., M.S., and S.J. analyzed the data. C.L. and M.S. wrote the paper with S.J., V.M.Z. contributing to revisions. M.S. and V.M.Z. provided funding acquisition and project supervision.

COMPETING INTERESTS

C.L. and M.S. are inventors for US patent application 17/959744 which has been filed on the partial basis of this work.

TABLES

Table 1. The number of electrons needed to fully oxidize a surface adsorbate to CO_2 (N) for several possible C_1 surface species.

Adsorbate Structure	N
*CO	2
*CHO or *COH	3
*C	4
*CH	5

FIGURES

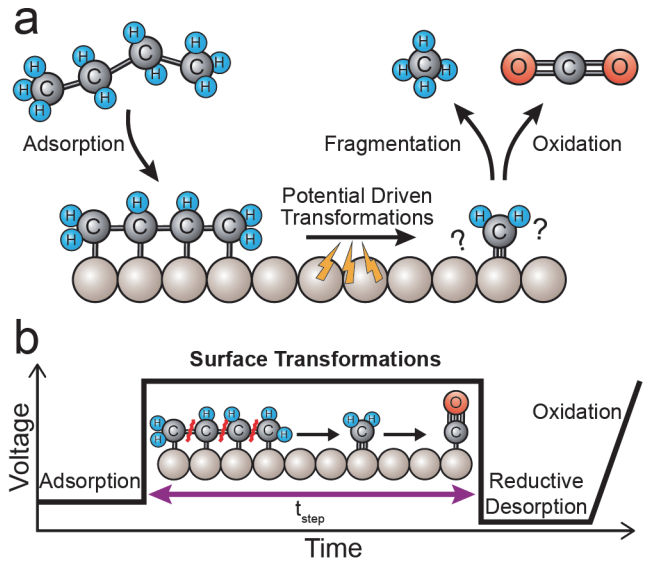

Figure 1. EC-MS interrogation of alkane fragmentation and oxidation branchpoint (a) Illustration of the possible electrocatalytic reaction pathways of butane on a Pt electrode leading to either fragmentation or oxidation. (b) Schematic of the time dependent applied potential profile used to study butane adsorption, C−C bond cleavage, and the subsequent reductive desorption or total oxidation of the resulting surface species.

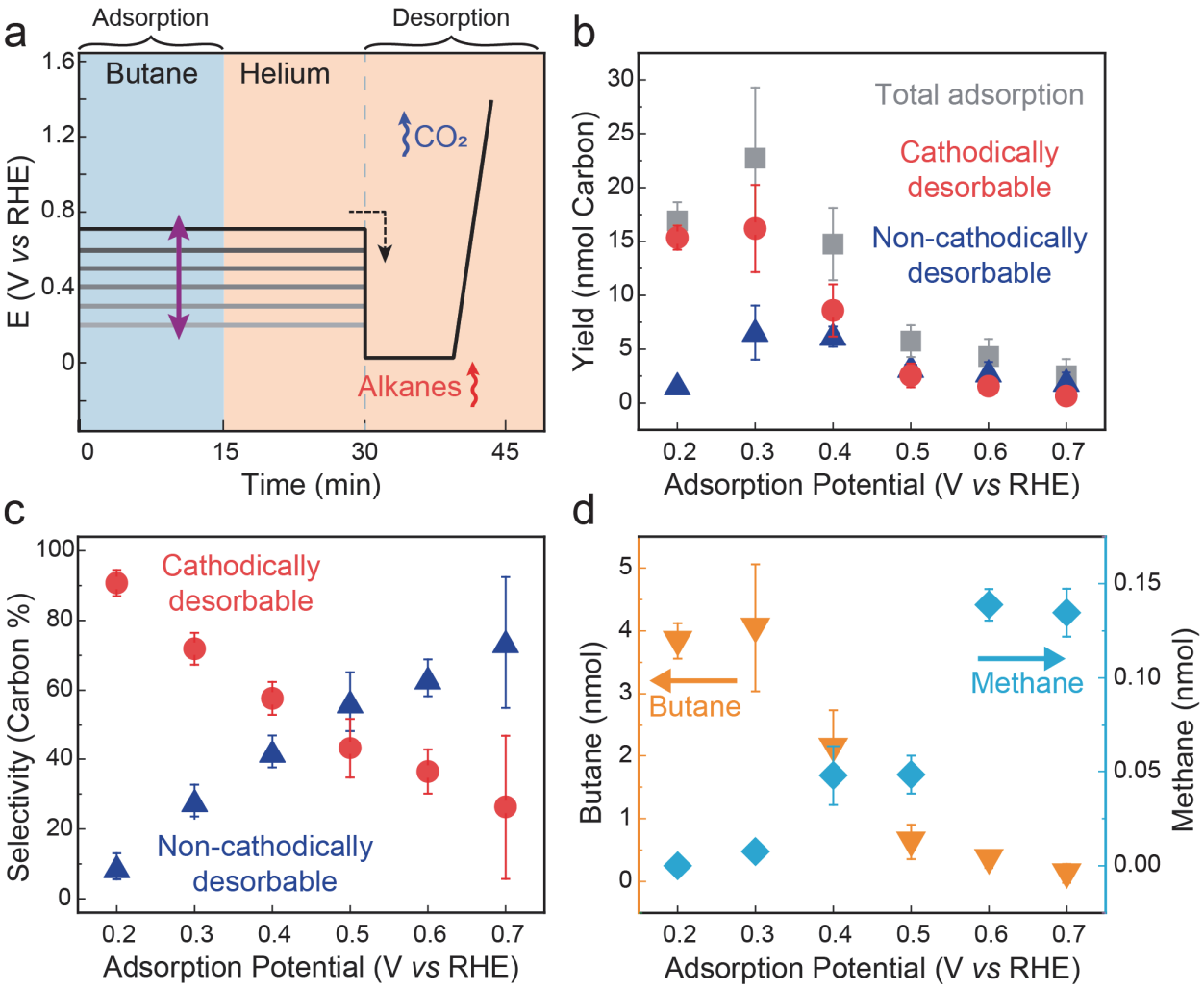

Figure 2. Potential dependence of butane adsorption and fragmentation on Pt (a) Potential program for butane adsorption at 0.2-0.7 V followed by reductive and oxidative desorption. (b) Potential dependent yields of reductively and oxidatively desorbed products on a carbon basis. (c) Potential dependent selectivity between reductively and oxidatively desorbed products on a carbon basis. (d) Methane and butane yields produced upon reductive desorption at 0.05 V following 15 min butane adsorption at varying potentials. All points are the average of at least three independent trials with error bars indicating the standard deviation. The results of individual trials are shown in Supplementary Figures 36-38.

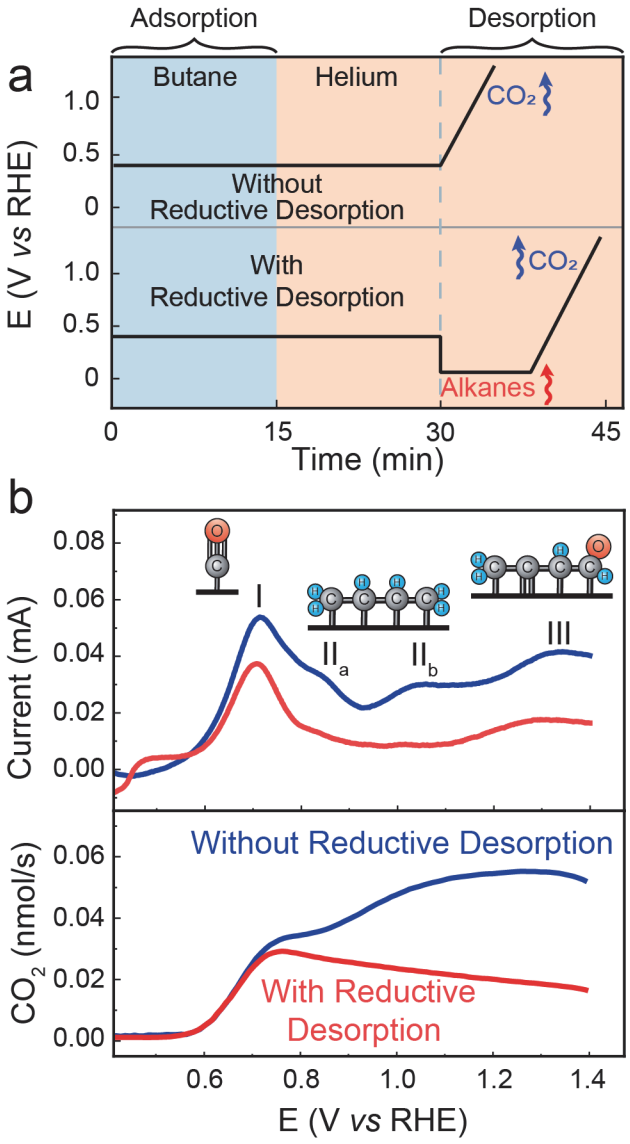

Figure 3. Oxidative stripping of butane-derived adsorbates (a) Potential program for the adsorption of butane at 0.4 V and subsequent stripping of surface species either with (red) or without (blue) a preceding reductive desorption step. (b) Difference in current and CO_2 produced during the 5 mV/s oxidative stripping of butane adsorbates after adsorption at 0.4 V and a corresponding experiment under He with and without a reductive desorption step prior to stripping. The proposed structures of the surface species are shown above the corresponding peak. The structure of species III is shown as a possible structure containing the proposed dehydrogenated and oxygenated characteristics discussed but the exact composition requires further investigation.

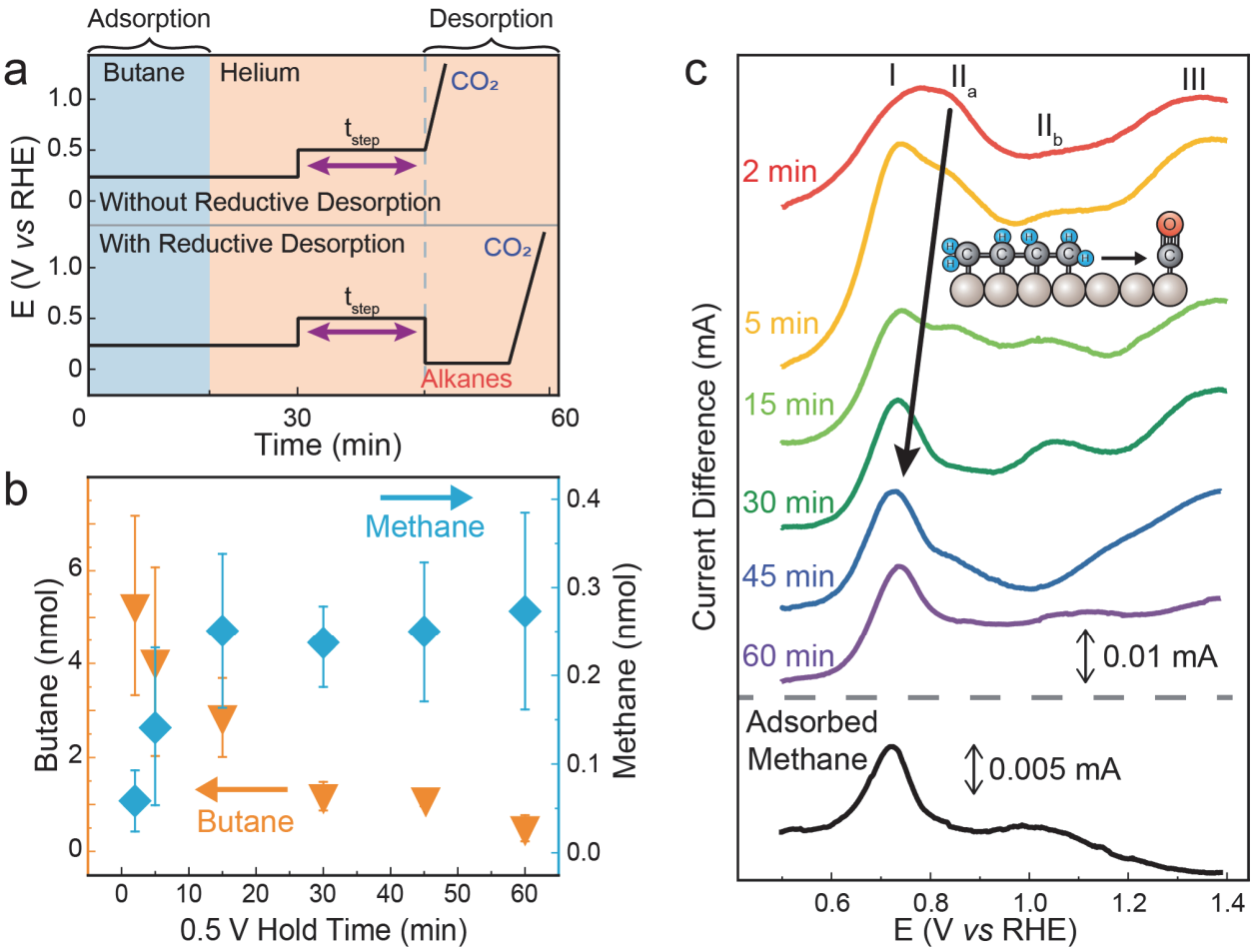

Figure 4. Potential induced transformation of pre-adsorbed butane (a) Potential program for butane adsorption at 0.2 V followed by a hold at 0.5 V *vs* RHE and oxidative stripping with or without a reductive desorption step at 0.05 V. (b) Methane and butane yields produced upon reductive desorption after butane adsorption and potential holds of varying duration at 0.5 V *vs* RHE. All points are the average of at least three independent trials with error bars indicating one standard deviation. All individual trials are shown in Supplementary Figure 39. (c) Oxidative stripping curves obtained after adsorbing butane at 0.2 V then applying a 0.5 V *vs* RHE hold of varying duration or adsorbing methane at 0.3 V *vs* RHE. All curves collected without a prior reductive desorption step.

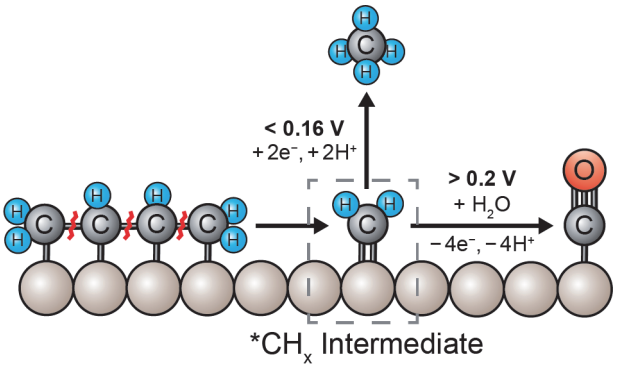

Figure 5. Proposed bifurcation between butane fragmentation and oxidation Schematic of the proposed branch point between alkane oxidation and fragmentation involving a *CH_x intermediate.

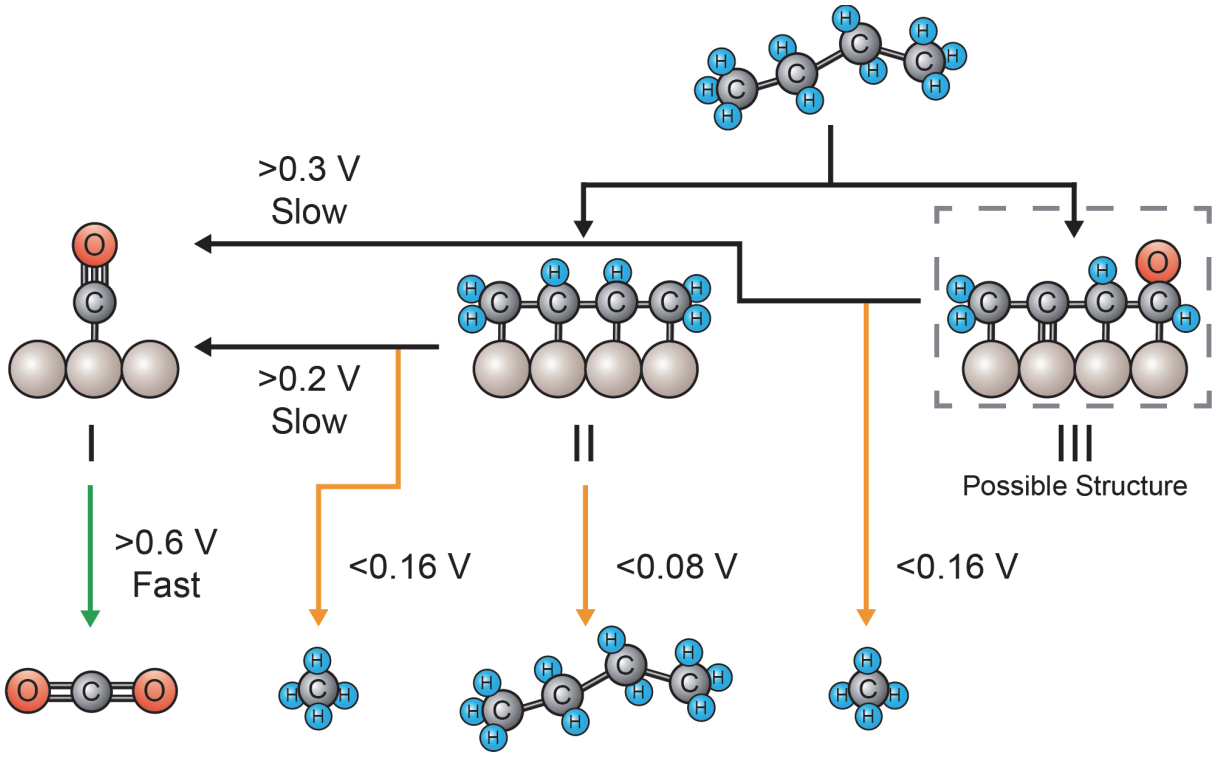

Figure 6. Reaction network of butane oxidation and fragmentation Proposed potential driven surface reactivity of butane on platinized Pt leading to the desorption of methane, butane, and CO_2.

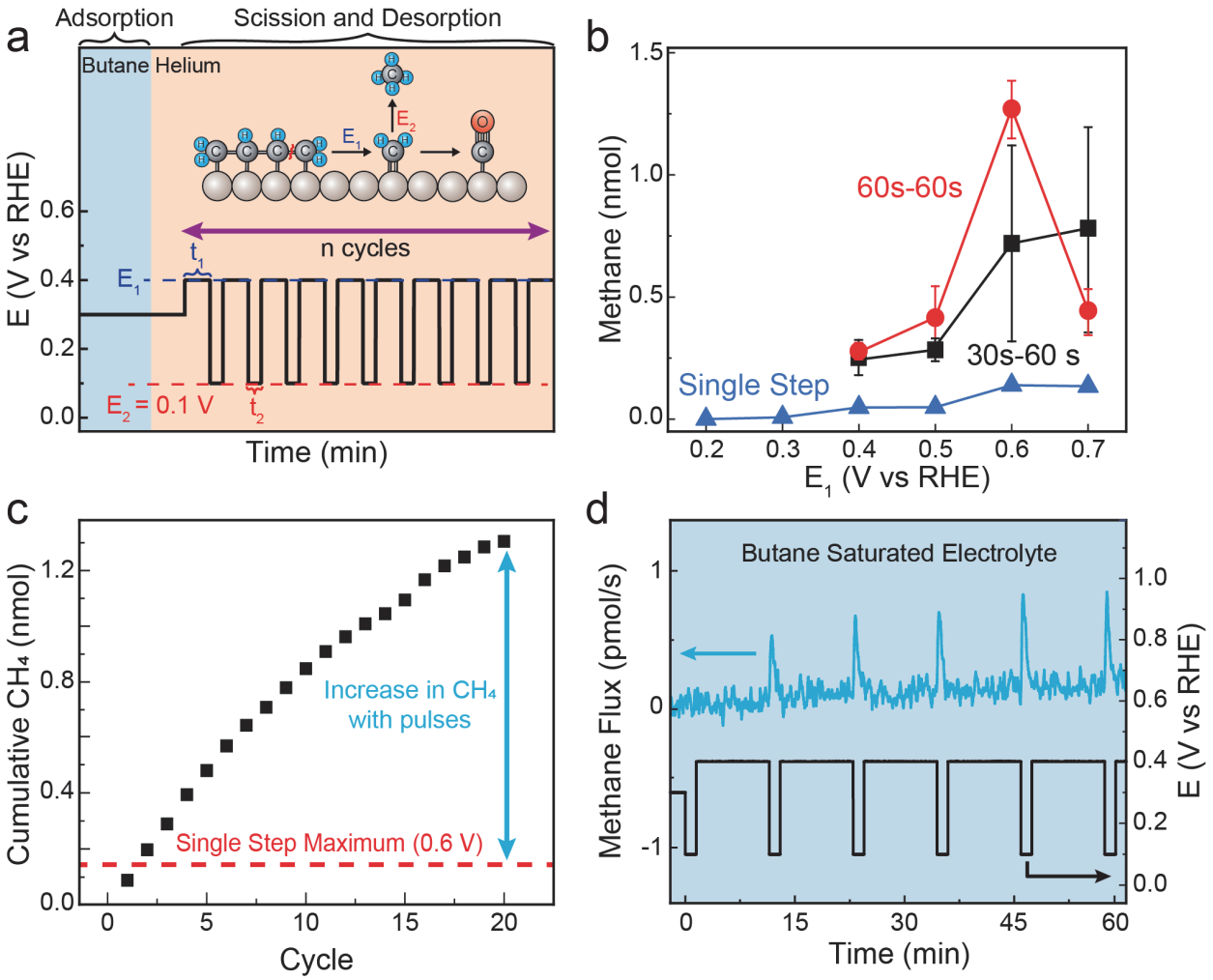

Figure 7. Pulsed potential program for increased methane generation (a) Potential program for repeated generation of and desorption of methane from butane adsorbed at 0.3 V for 15 min. E_1 varied between 0.4 and 0.7 V. (b) Methane yield from 20 cycles of fragmentation at an E_1 (as defined in panel a) of 0.4 to 0.7 V and desorption at 0.1 V compared to the methane yield after a single 15 min fragmentation step at the corresponding E_1 potential. The pulsed potential conditions are labeled as t_1-t_2 as defined in panel a. Each point corresponds to the average of at least three independent trials with error bars showing one standard deviation. (c) The cumulative methane yield over the first 20 cycles of the *60s-60s* potential program at 0.6 V compared to the single step yield. Triplicates shown in Supplementary Figure 40. (d) The methane flux and potential during repeated potential oscillation in a butane saturated electrolyte showing repeatable methane desorption. Additional cycles shown in Supplementary Figure 41.

REFERENCES

1. Xia, R., Overa, S. & Jiao, F. Emerging Electrochemical Processes to Decarbonize the Chemical Industry. *J. Am. Chem. Soc. Au* **2**, 1054–1070 (2022).
2. National Academy of Sciences, National Academy of Engineering & National Research Council. *America's Energy Future: Technology and Transformation*. *America's Energy Future: Technology and Transformation* (National Academies Press, 2009).
3. Schiffer, Z. J. & Manthiram, K. Electrification and Decarbonization of the Chemical Industry. *Joule* **1**, 10–14 (2017).
4. Daehn, K.; Basuhi, R.; Gregory, J.; Berlinger, M.; Somjit, V.; Olivetti, E. A. Innovations to decarbonize materials industries. *Nat. Rev. Mat. 7*, 275–294 (2021).
5. Chen, B. & Sargent, E. H. What does net zero by 2050 mean to the solar energy materials researcher? *Matter* **5**, 1322–1325 (2022).
6. Van Geem, K. M., Galvita, V. V. & Marin, G. B. Making chemicals with electricity. *Science* **364**, 734–735 (2019).
7. Lopez, G., Artetxe, M., Amutio, M., Bilbao, J. & Olazar, M. Thermochemical routes for the valorization of waste polyolefinic plastics to produce fuels and chemicals. A review. *Renew. Sust. Energ. Rev.* **73**, 346–368 (2017).
8. Vollmer, I. *et al.* Beyond Mechanical Recycling: Giving New Life to Plastic Waste. *Angew. Chem., Int. Ed.* **59**, 15402–15423 (2020).
9. Häußler, M., Eck, M., Rothauer, D. & Mecking, S. Closed-loop recycling of polyethylene-like materials. *Nature* **590**, 423–427 (2021).
10. Lucky, C., Wang, T. & Schreier, M. Electrochemical Ethylene Oxide Synthesis from Ethanol. *ACS Energy Lett.* **7**, 1316–1321 (2022).
11. Goetz, M. K. K., Bender, M. T. & Choi, K. S. Predictive control of selective secondary alcohol oxidation of glycerol on NiOOH. *Nat. Comm.* **13**, 1–10 (2022).
12. Luo, H. *et al.* Progress and Perspectives in Photo- and Electrochemical-Oxidation of Biomass for Sustainable Chemicals and Hydrogen Production. *Adv. Energy Mater.* **11**, 2101180 (2021).
13. You, B., Liu, X., Jiang, N. & Sun, Y. A General Strategy for Decoupled Hydrogen Production from Water Splitting by Integrating Oxidative Biomass Valorization. *J. Am. Chem. Soc.* **138**, 13639–13646 (2016).
14. Zhu, C., Ang, N. W. J., Meyer, T. H., Qiu, Y. & Ackermann, L. Organic Electrochemistry: Molecular Syntheses with Potential. *ACS Cent. Sci.* **7**, 415–431 (2021).
15. Newhouse, T. & Baran, P. S. If C-H bonds could talk: Selective C-H bond oxidation. *Angew. Chem., Int. Ed.* **50**, 3362–3374 (2011).
16. Yan, M., Kawamata, Y. & Baran, P. S. Synthetic Organic Electrochemical Methods Since 2000 : On the Verge of a Renaissance. *Chem. Rev.* **117**, 13230–13319 (2017).
17. Peters, B. K. *et al.* Scalable and safe synthetic organic electroreduction inspired by Li-ion battery chemistry. *Science* **363**, 838–845 (2019).
18. Park, S., Vohs, J. M. & Gorte, R. J. Direct oxidation of hydrocarbons in a solid-oxide fuel cell. *Nature* **404**, 265–267 (2000).
19. Hibino, T. *et al.* A low-operating-temperature solid oxide fuel cell in hydrocarbon-air mixtures. *Science* **288**, 2031–2033 (2000).
20. Brummer, S. B. & Turner, M. J. Oxidation and Adsorption of Hydrocarbons on Noble Metal Electrodes. III. CH-Type and O-Type Intermediates during the Oxidative Adsorption of Propane on Platinum. *J. Phys. Chem.* **71**, 2825–2837 (1967).

21. Barger Jr, H. J. & Coleman, A. J. Hydrogen-Deuterium Exchange of Propane on a Fuel-Cell Electrode. *J. Phys. Chem.* **72**, 2285–2286 (1968).
22. Shropshire, J. A. & Horowitz, H. H. Adsorption and Electrooxidation of Butane on Platinum Black in H_2SO_4. *J. Electrochem. Soc.* **113**, 490–495 (1966).
23. Bockris, J. O., Gileadi, E. & Stoner, G. E. The Anodic Oxidation of Saturated Hydrocarbons. A Mechanistic Study. *J. Phys. Chem.* **73**, 427–434 (1969).
24. Grubb, W. T. & Lazarus, M. E. Carbon Dioxide Determination during the Galvanostatic Oxidation of Adsorbed Propane Intermediates. *J. Electrochem. Soc.* **114**, 360–361 (1967).
25. Brummer, S. B., Ford, J. I. & Turner, M. J. The Adsorption and Oxidation of Hydrocarbons on Noble Metal Electrodes. I. Propane Adsorption on Smooth Platinum Electrodes. *J. Phys. Chem.* **69**, 3424–3433 (1965).
26. Brummer, S. B. & Turner, M. J. The Adsorption and Oxidation of Hydrocarbons on Noble Metal Electrodes; Propane Adsorption on Smooth Pt at Elevated Temperatures. in *Hydrocarbon Fuel Cell Technology* (ed. Baker, B. S.) 408–428 (Academic Press Inc., 1965).
27. Niedrach, L. W., Gilman, S. & Weinstock, I. Studies of Hydrocarbon Fuel Cell Anodes by the Multipulse Potentiodynamic Method I. Behavior of Ethane on Conducting-Porous-Teflon Electrodes. *J. Electrochem. Soc.* **112**, 1161–1166 (1965).
28. Gilman, S. Studies of Hydrocarbon Surface Processes by the Multipulse Potentiodynamic Method Part 1.-Kinetics and Mechanisms of Ethane Adsorption on Platinum. *J. Chem. Soc., Faraday trans.* **61**, 2546–2560 (1965).
29. Lamy, C. *et al.* Recent advances in the development of direct alcohol fuel cells (DAFC). *J. Power Sources* **105**, 283–296 (2002).
30. Li, N. H., Sun, S. G. & Chen, S. P. Studies on the role of oxidation states of the platinum surface in electrocatalytic oxidation of small primary alcohols. *J. Electroanal. Chem.* **430**, 57–67 (1997).
31. Puthiyapura, V. K., Brett, D. J. L., Russell, A. E., Lin, W. F. & Hardacre, C. Biobutanol as Fuel for Direct Alcohol Fuel Cells-Investigation of Sn-Modified Pt Catalyst for Butanol Electro-oxidation. *ACS Appl. Mater. Interfaces* **8**, 12859–12870 (2016).
32. Rodrigues, I. D. A., De Souza, J. P. I., Pastor, E. & Nart, F. C. Cleavage of the C-C bond during the electrooxidation of 1-propanol and 2-propanol: Effect of the Pt morphology and of codeposited Ru. *Langmuir* **13**, 6829–6835 (1997).
33. Li, N. H. & Sun, S. G. In situ FTIR spectroscopic studies of the electrooxidation of C4 alcohol on a platinum electrode in acid solutions Part I. Reaction mechanism of 1-butanol oxidation. *J. Electroanal. Chem.* **436**, 65–72 (1997).
34. Pastor, E. *et al.* Spectroscopic investigations of C_3 primary alcohols on platinum electrodes in acid solutions. Part I. n-propanol. *J. Electroanal. Chem.* **350**, 97–116 (1993).
35. Brummer, S. B. Oxidation and Adsorption of Hydrocarbons on Noble Metal Electrodes VI. A Discussion of the Mechanism of Saturated Hydrocarbon Oxidation on Platinum. in *Fuel Cell Systems - II* (ed. Gould, R. F.) 223–230 (American Chemical Society, 1969).
36. Bruckenstein, S. & Comeau, J. Electrochemical Mass Spectrometry Part 1 .-Preliminary Studies of Propane Oxidation on Platinum. *J. Chem. Soc., Faraday trans.* **91**, 285–292 (1973).
37. Barger Jr., H. J. & Savitz, M. L. Chemical Identification of Adsorbed Species in Fuel Cell Reactions I. Propane Oxidation. *J. Electrochem. Soc.* **115**, 686–690 (1968).

38. Bruckenstein, S., Reidhammer, T. M. & Jureviciute, I. Electrochemical mass spectrometric study of 2-methyl-propane adsorbates formed at platinum in phosphoric acid at 105 °C. *J. Electroanal. Chem.* **552**, 35–43 (2003).
39. Solis, V., Castro Luna, A., Triaca, W. E. & Arvfa, A. J. The Electrosorption and the Potentiodynamic Electrooxidation of Ethane on Platinum at Different Temperatures. *J. Electrochem. Soc.* **128**, 2115–2122 (1981).
40. Bakshi, H. B.; Lucky, C.; Chen, H. S.; Schreier, M. Electrocatalytic Scission of Unactivated $C(sp^3)$-$C(sp^3)$ Bonds through Real-Time Manipulation of Surface-Bound Intermediates. *J. Am. Chem. Soc.* **2023**, *145*, 13742–13749.
41. Trimarco, D. B. *et al.* Enabling real-time detection of electrochemical desorption phenomena with sub-monolayer sensitivity. *Electrochim. Acta.* **268**, 520–530 (2018).
42. Baltruschat, H. Differential electrochemical mass spectrometry. *J. Am. Soc. Mass Spectrom.* **15**, 1693–1706 (2004).
43. Boyd, M. J. *et al.* Electro-Oxidation of Methane on Platinum under Ambient Conditions. *ACS Catal.* **9**, 7578–7587 (2019).
44. Gurses, S. M., Kronawitter, C. X. Electrochemistry of the Interaction of Methane with Platinum at Room Temperature Investigated through Operando FTIR Spectroscopy and Voltammetry. *J. Phys. Chem. C* **125**, 2944–2955 (2021).
45. López-Cudero, A., Cuesta, A. & Gutiérrez, C. Potential dependence of the saturation CO coverage of Pt electrodes: The origin of the pre-peak in CO-stripping voltammograms. Part 1: Pt(111). *J. Electroanal. Chem.* **579**, 1–12 (2005).
46. Cuesta, A. *et al.* Potential dependence of the saturation CO coverage of Pt electrodes: The origin of the pre-peak in CO-stripping voltammograms. Part 3: Pt(poly). *J. Electroanal. Chem.* **586**, 184–195 (2006).
47. Housmans, T. H. M., Hermse, C. G. M. & Koper, M. T. M. CO oxidation on stepped single crystal electrodes: A dynamic Monte Carlo study. *J. Electroanal. Chem.* **607**, 69–82 (2007).
48. Voglis, C. & Lagaris, I. E. A Rectangular Trust Region Dogleg Approach for Unconstrained and Bound Constrained Nonlinear Optimization. in *WSEAS Int. Conf. Appl. Math.* 7 (2004).
49. Horányi, G. On the adsorption of organic compounds on platinized platinum electrodes. *J. Electroanal. Chem.* **51**, 163–178 (1974).
50. Flannery, R. J. & Walker, D. C. Using Radiotracers to Study Hydrocarbon Adsorption Directly at Electrodes. in *Hydrocarbon Fuel Cell Technology* (ed. Baker, B. S.) 335–348 (Academic Press, 1965).
51. Ojha, K., Arulmozhi, N., Aranzales, D. & Koper, M. T. M. Double Layer at the Pt(111)–Aqueous Electrolyte Interface: Potential of Zero Charge and Anomalous Gouy–Chapman Screening. *Angew. Chem., Int. Ed.* **59**, 711 (2020).
52. Piersma, B. J. Organic Adsorption at Electrodes. in *Electrosorption* (ed. Gileadi, E.) 19–49 (Plenum Press, 1967).
53. Lucky, C. & Schreier, M. Mind the Interface: The Role of Adsorption in Electrocatalysis. *ACS Nano* (2024) doi:10.1021/ACSNANO.3C09523.
54. Beltowska-Brzezinska, M., Luczak, T., Baltruschat, H. & Müller, U. Propene oxidation and hydrogenation on a porous platinum electrode in acidic solution. *J. Phys. Chem. B* **107**, 4793–4800 (2003).
55. Gootzen, J. F. E., Wonders, A. H., Visscher, W. & Van Veen, J. A. R. Adsorption of C_3 alcohols, 1-butanol, and ethene on platinized platinum as studied with FTIRS and DEMS. *Langmuir* **13**, 1659–1667 (1997).

56. Lucky, C., Fuller, L. & Schreier, M. Determining the potential-dependent identity of methane adsorbates at Pt electrodes using EC-MS. *Catal. Sci. Technol.* **14**, 353-361 (2024).
57. Niedrach, L. W. Galvanostatic and Volumetric Studies of Hydrocarbons Adsorbed on Fuel Cell Anodes. *J. Electrochem. Soc.* **111**, 1309–1317 (1964).
58. Giner, J. Electrochemical reduction of CO_2 on platinum electrodes in acid solutions. *Electrochim. Acta* **8**, 857–865 (1963).
59. Schmiemann, U., Müller, U. & Baltruschat, H. The influence of the surface structure on the adsorption of ethene, ethanol and cyclohexene as studied by DEMS. *Electrochim. Acta* **40**, 99–107 (1995).
60. Beltowska-Brzezinska, M., Luczak, T., Maczka, M., Baltruschat, H. & Müller, U. Ethyne oxidation and hydrogenation on porous Pt electrode in acidic solution. *J. Electroanal. Chem.* **519**, 101–110 (2002).
61. Arenz, M. *et al.* The effect of the particle size on the kinetics of CO electrooxidation on high surface area Pt catalysts. *J. Am. Chem. Soc.* **127**, 6819–6829 (2005).
62. Yan, Y. G. *et al.* Study of CO oxidation on polycrystalline Pt electrodes in acidic solution by ATR-SEIRAS. *J. Phys. Chem. C* **115**, 16378–16388 (2011).
63. Löffler, T. & Baltruschat, H. Temperature dependent formation of multiple adsorption states from ethene at polycrystalline Pt and Pt(111) electrodes studied by differential electrochemical mass spectrometry. *J. Electroanal. Chem.* **554–555**, 333–344 (2003).
64. Gopeesingh, J. *et al.* Resonance-promoted formic acid oxidation via dynamic electrocatalytic modulation. *ACS Catal.* **10**, 9932–9942 (2020).
65. Timoshenko, J. *et al.* Steering the structure and selectivity of CO2 electroreduction catalysts by potential pulses. *Nat. Catal.* **5**, 259–267 (2022).
66. Casebolt, R., Levine, K., Suntivich, J. & Hanrath, T. Pulse check: Potential opportunities in pulsed electrochemical CO_2 reduction. *Joule* **5**, 1987–2026 (2021).
67. Chen, W. *et al.* Pulse potential mediated selectivity for the electrocatalytic oxidation of glycerol to glyceric acid. *Nat. Commun.* **15**, 1–11 (2024).
68. Blanco, D. E., Lee, B. & Modestino, M. A. Optimizing organic electrosynthesis through controlled voltage dosing and artificial intelligence. *Proc. Natl. Acad. Sci. USA* **116**, 17683–17689 (2019).
69. Lee, C. W., Cho, N. H., Nam, K. T., Hwang, Y. J. & Koun Min, B. Cyclic two-step electrolysis for stable electrochemical conversion of carbon dioxide to formate. *Nat. Commun.* **10**, 3919 (2019).
70. Kim, D., Zhou, C., Zhang, M. & Cargnello, M. Voltage cycling process for the electroconversion of biomass-derived polyols. *Proc. Natl. Acad. Sci. USA* **118**, e2113382118 (2021).
71. Fedkiw, P. S., Traynelis, C. L. & Wang, S.-R. Pulsed-Potential Oxidation of Methanol. *J. Electrochem. Soc.* **135**, 2459–2465 (1988).
72. Adžić, R. R., Popov, K. I. & Pamić, M. A. Acceleration of electrocatalytic reactions by pulsation of potential: Oxidation of formic acid on Pt and Pt/Pb_{ads} electrodes. *Electrochim. Acta* **23**, 1191–1196 (1978).
73. Ghumman, A. & Pickup, P. G. Efficient electrochemical oxidation of ethanol to carbon dioxide in a fuel cell at ambient temperature. *J. Power Sources* **179**, 280–285 (2008).
74. Gasteiger, H. A., Markovic, N. M. & Ross, P. N. Electrooxidation of CO and H_2/CO Mixtures on a Well-Characterized Pt_3Sn Electrode Surface. *J. Phys. Chem.* **99**, 8945–8949 (1995).

75. Lin, W. F., Iwasita, T. & Vielstich, W. Catalysis of CO Electrooxidation at Pt, Ru, and PtRu Alloy. An in Situ FTIR Study. *J. Phys. Chem. B* **103**, 3250-3257 (1999).
76. Stamenković, V. R. *et al.* Surface chemistry on bimetallic alloy surfaces: Adsorption of anions and oxidation of CO on $Pt_3Sn(111)$. *J. Am. Chem. Soc.* **125**, 2736–2745 (2003).
77. Huang, H., Blackman, O. F., Celorrio, V. & Russell, A. E. Isolating the contributions of surface Sn atoms in the bifunctional behaviour of PtSn CO oxidation electrocatalysts. *Electrochim. Acta* **390**, 138811 (2021).
78. Dupont, C., Jugnet, Y. & Loffreda, D. Theoretical evidence of PtSn alloy efficiency for CO oxidation. *J. Am. Chem. Soc.* **128**, 9129–9136 (2006).
79. Almithn, A. & Hibbitts, D. Comparing Rate and Mechanism of Ethane Hydrogenolysis on Transition-Metal Catalysts. *J. Phys. Chem. C* **123**, 5421–5432 (2019).
80. Huynh, T. T., Dang, N. N. & Pham, H. Q. Bimetallic PtIr nanoalloy on TiO_2-based solid solution oxide with enhanced oxygen reduction and ethanol electro-oxidation performance in direct ethanol fuel cells. *Catal. Sci. Technol.* **11**, 1571–1579 (2021).
81. Dang, Q. *et al.* Iridium metallene oxide for acidic oxygen evolution catalysis. *Nat. Comm.* **12**, 1–10 (2021).
82. Feltham, A. M. & Spiro, M. Platinized platinum electrodes. *Chem. Rev.* **71**, 177–193 (1971).
83. Herrero, E.; Buller, L. J.; Abruña, H. D. Underpotential Deposition at Single Crystal Surfaces of Au, Pt, Ag and Other Materials. *Chem. Rev.* **101**, 1897–1930 (2001).